Numerical simulation of the octorotor flying car in sudden rotor stop

Naoya Takahashi[1][✉], Ritsuka Gomi[1], Ayato Takii[1,2], Masashi Yamakawa[1],

Shinichi Asao[3] and Seiichi Takeuchi[3]

[1] Kyoto Institute of Technology, Matsugasaki, Sakyo-ku, Kyoto 606-8585, Japan

[2] RIKEN Center for Computational Science, 7-1-26 Minatojima-minami-machi,

Chuo-ku, Kobe, Hyogo 650-0047, Japan

[3] College of Industrial Technology, 1-27-1, Amagasaki, Hyogo 661-0047, Japan

`m2623017@edu.kit.ac.jp`

Abstract. Currently, manned drones, also known as flying cars, are attracting attention, but due to legal restrictions and fear of accidents, it is difficult to fly them. We therefore present a numerical simulation of the sudden stop of the rotor of an octrotor flying car. In this paper, we consider the interaction between fluid and rigid-body in a 6-degrees of freedom flight simulation of a flying car. For the purpose, the attitude of the aircraft is determined based on the force generated from the flow field around the aircraft due to the rotation of the rotor. The motion of the aircraft is obtained from the equations of motion of translation and rotation, and Newton's equation of motion and Euler's equation of rotation are used. A multi-axis sliding mesh is adopted for the rotation of the rotor, and calculations with multiple rotating bodies in the computational grid are performed. In addition, we use the motion computational domain (MCD) method to represent the free motion of the octrotor flying car by the motion computational domain itself. Using the above method, we will show the appropriate rotation method from various rotor stop patterns, demonstrate the safety of the octrotor flying car, and clarify the behavior of the aircraft and the surrounding flow field.

Keywords : CFD, moving grids, coupled computation, flying car.

1   Introduction

In recent years, the development of flying cars that can travel in airspace has been the focus of attention as a revolution in mobility. Flying cars, especially VTOL (Vertical Take Off and Landing), are new vehicles that fly using multiple rotors. In addition, the shape of the airframe is not predetermined, and various mechanisms are being evaluated and compared [1]. Most VTOL are electric driven nowadays, called eVTOL,

which are environmentally friendly and can travel between cities. However, the safety of flying cars must be improved for inter-city travel. Aerodynamic performance is an important factor in aircraft, and many studies on drag and lift forces on aircraft bodies have been reported [2]. Aerodynamic around the rotor have been studied by Seokkwan Yoon et al [3] using numerical simulations. However, most of these studies are based on steady-state flight tests and wind tunnel tests. In actual flight, steady-state conditions are rare and the phenomena are more complex. Although flight tests of actual flying vehicles are being conducted around the world, legal regulations and the fear of accidents prevent easy flight. In addition, many tests with actual aircraft are required to improve the safety of the vehicle, and the time and cost for development are likely to increase. Therefore, it is necessary to establish a more practical flight prediction method using numerical method.

Unmanned drones have often become inoperable and crashed due to damage to the propeller parts or external disturbances such as wind [4]. Unmanned drones rarely cause damage if the location of the crash is taken into account, but manned drones must be able to land without losing their posture in an emergency because a person is aboard the drone. Therefore, even if one rotor stops, the flying car needs to maintain hovering with the lift force of the other rotors. However, it leads to crash accidents because it is difficult to control the attitude when the rotor suddenly stops. In order to solve this problem, it is first necessary to clarify how the flying car is affected by the air flow when the rotor suddenly stops, and how the flight behavior of the car is affected by that. However, in the flight simulation of the flying car, it is necessary to couple the interaction between the flight dynamics, which deals with the movement of the flying car, and the fluid dynamics, which handles the fluid around the flying car. This numerical simulation is very difficult to perform because it involves such a very complicated moving boundary problem. In contrast, the authors have proposed a method that combines the MCD (Moving Computational Domain) method [5] based on the unstructured mesh finite volume method and the multi-axis sliding mesh method [6]. The MCD method applies the finite volume method to a 4-dimensional inspection volume and discretizes it, enabling calculations while strictly satisfying geometric conservation laws. In addition, the multi-axis sliding mesh method can represent motions such as rotation by forming computational domains divided by regions with different states of motion. Yamakawa et al. [7] used this method to analyze the submarine flow and clarify the effect of the shape of the free water surface.

It is thought that the flight behavior of the flying car is able to be simulated by applying the multi-axis sliding mesh method to multiple rotor sections that are independent of each other. In this study, flight simulations of the octorotor flying car with fluid and rigid-body interaction are performed to investigate the behavior of the flying car in the case of sudden stop of rotors. In addition, as a method to maintain stable hovering when the rotor suddenly stops, we examine the effectiveness of the method of rotating other rotors in reverse.

2   Numerical Approach

2.1   Governing Equation

In present work, since the flow around the propeller is included, the Reynolds number is approximately 3,000,000 and the maximum Mach number is 0.55. Therefore, it was treated as a compressible fluid and the Euler equations were used without considering viscosity. In addition, the ideal gas equation of state was used as the governing equation. The governing equations are shown in Equations. (1)-(3).

$$\frac{\partial \boldsymbol{q}}{\partial t} + \frac{\partial \boldsymbol{E}}{\partial x} + \frac{\partial \boldsymbol{F}}{\partial y} + \frac{\partial \boldsymbol{G}}{\partial z} = 0, \tag{1}$$

$$\boldsymbol{q} = \begin{bmatrix} \rho \\ \rho u \\ \rho v \\ \rho w \\ e \end{bmatrix}, \boldsymbol{E} = \begin{bmatrix} \rho u \\ \rho u^2 + p \\ \rho uv \\ \rho uw \\ u(e + p) \end{bmatrix}, \boldsymbol{F} = \begin{bmatrix} \rho v \\ \rho uv \\ \rho v^2 + p \\ \rho vw \\ v(e + p) \end{bmatrix}, \boldsymbol{G} = \begin{bmatrix} \rho w \\ \rho uw \\ \rho vw \\ \rho w^2 + p \\ w(e + p) \end{bmatrix}, \tag{2}$$

$$p = (\gamma - 1)\left\{ e - \frac{1}{2}\rho(u^2 + v^2 + w^2) \right\}, \tag{3}$$

where $\boldsymbol{q}$ is the conserved quantity vector, and $\boldsymbol{E}$, $\boldsymbol{F}$, and $\boldsymbol{G}$ are the inviscid flux vectors in the x, y, and z directions, respectively. In addition, ρ is density, u, v, and w are velocities in the x, y, and z directions, respectively, p is pressure, and e is total energy per unit volume. The inviscid flux vectors are evaluated using Roe's velocity-difference separation [8] and MUSCL methods. Green-Gauss method and Hishida's van Leer-like limiter are used for variable reconstruction [9]. The specific heat ratio γ is assumed to be 1.4 in this study. The proposed model is simulated by means of a two-step rational Runge-Kutta numerical method.

2.2   Unstructured Moving-Grid Finite-Volume Method

This study investigates the behavior of the flying car when its rotor comes to a sudden stop. Conventionally, the flow field around the aircraft has been calculated by placing the object to be calculated at the center of the calculation and applying uniform flow. However, for this case, a uniform flow cannot reproduce free motion because the aircraft's attitude is expected to change significantly due to the sudden stop of the rotor. Therefore, a moving-grid finite volume method is used, in which the computational domain can be moved by the motion of the aircraft. The unstructured moving-grid finite volume method applies the finite volume method to a four-dimensional inspection volume, including time and space, and discretizes it. Therefore, even if the lattice is moved, the calculation can be performed while strictly

satisfying the geometric conservation law. As shown in Fig.1, this method can reproduce free motion without restrictions.
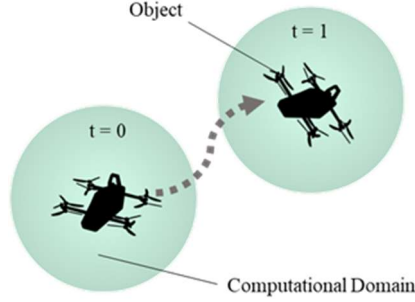

Fig.1 Moving Computational Domain Method

2.3 Sliding Mesh Approach

The rotor section of the flying car requires a separate computational domain, unlike the kinematic state of the airframe. Therefore, the sliding mesh method, which enables the transfer of physical quantities across multiple computational domains, is used to calculate the fluid flow. This method slides the mesh itself at a specific interface, and the volume does not change due to deformation of the mesh. As shown in Fig.2, one element is in contact with one or more other elements on the sliding surface, and the interpolation of physical quantities between regions is performed using Equation. (4).

$$\boldsymbol{q}_{bi} = \frac{1}{S_i} \sum_{j \in i} \boldsymbol{q}_j S_{ij}, \qquad (4)$$

where $\boldsymbol{q}_{bi}$ is the physical quantity possessed by the virtual cell in cell i, $\boldsymbol{q}_j$ is the physical quantity possessed by cell j, S_{ij} is the overlapped area of cell i and cell j, and S_i is the area of cell i in the sliding plane. In this study, all computational domains consist of nine regions, one around the aircraft and eight in the rotor section, and the rotor rotation is reproduced using the sliding mesh method.
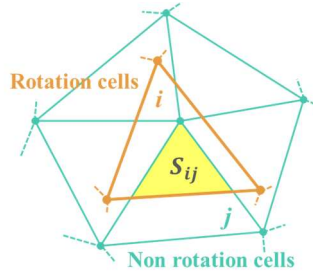

Fig.2 Sliding Mesh Method

2.4   Coupled Computation

In this study, the position and attitude of the flying car are determined by weakly coupled calculations that take into account the interaction between the fluid and the rigid-body of the aircraft. The motion of the aircraft can be obtained from the equations of motion for translation and rotation, and Newton's equation of motion and Euler's equation of rotation are used. Newton's equation of motion is shown in Equation. 5, and Euler's equation of rotation is shown in Equation. 6.

$$m\frac{d^2\boldsymbol{r}}{dt^2} = \boldsymbol{F}, \tag{5}$$

$$I\frac{d\boldsymbol{\omega}}{dt} + \boldsymbol{\omega} \times I\boldsymbol{\omega} = \boldsymbol{T}, \tag{6}$$

where m is the mass of the aircraft, $\boldsymbol{r}$ is the position vector of the center of the aircraft, and $\boldsymbol{F}$ is the force vector. I is the inertia tensor written in matrix form, $\boldsymbol{\omega}$ is the angular velocity vector, and $\boldsymbol{T}$ is the torque vector around the aircraft center. The force and torque are calculated from the pressure applied to the surface of the aircraft.

3   Flight Simulation of Flying Car

3.1   Computational Model

The computational model (Fig.3) is based on SkyDrive's SD-03 [10], for which actual flight experiments were conducted. Table 1 shows the specifications of the computational model. The rotor, arranged on the same axis, is a contra-rotating type. The model was created with the aircraft size of 4[m] as the representative length and the computational model as 1[-]. The computational model is an unstructured mesh and was created using MEGG3D [11][12]. The total number of elements is about 3,000,000, and the rotor part is about 120,000 by itself. In this study, a sliding mesh method was used to reproduce the rotation of the rotor. Therefore, as shown in Fig.4, the entire computational domain was constructed by fitting the rotor domain to the airframe domain.

Table.1   Specifications of the computational model

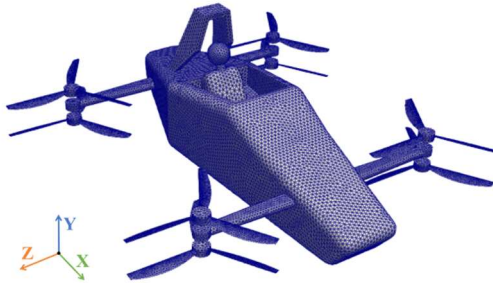|	
Aircraft weight	400 [kg]
Aircraft Sizes(x,y,z)	4, 2, 4 [m]
Number of rotors	8
Number of rotor blades	3
Hovering rotor speed	1930 [rpm]

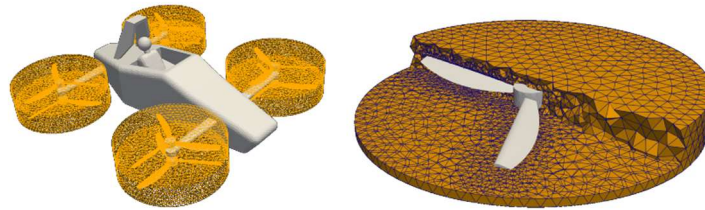**Fig.3** Computational surface grid

Fig.4 Sliding Mesh region and mesh around rotors

Fig.5 shows a cross-sectional view of the computational domain and a mesh cross section around the airframe of the flying car. The computational domain is a sphere with the computational target in the center. The size of the sphere is 30L, which is 30 times the size of the flying car.
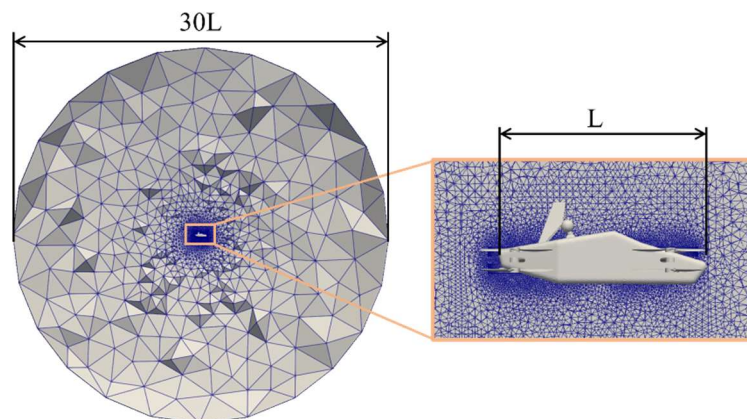

Fig.5 Computational Domain

3.2   Computational Conditions

Table 2 shows the initial values of variables and boundary conditions. The characteristic velocity and density are set to 340.29 [m/s] and 1.247 [kg/m^3], respectively. The variables are nondimensionalized by these characteristic values.

Table.2   Initial condition

ρ	1.0
p	$1.0 / \gamma$
u, v, w	0.0, 0.0, 0.0
Aircraft surface	Slip wall condition
Outer boundary	Riemann invariant boundary condition

3.3   Control Method

The rotor speed is controlled by PD control, which is widely used in the world. In this study, we conduct a numerical experiment in which the rotor is suddenly stopped and the flight attitude is forcibly broken on the simulation. In that case, it works to maintain the correct flight attitude by automatically controlling the rotation speed of other rotors. The rotation of the rotor is determined by the superposition of four manipulated variables: the throttle that controls altitude, the aileron that controls roll, the rudder that controls yaw, and the elevator that controls pitch. In order to hover, the target angles of roll, pitch, and yaw angle are all set to zero. The target altitude is set to 0.5[m]. After confirming that the roll, pitch, yaw angle, and altitude have reached their target values and that the motion is stable, the rotor is brought to the sudden stop. Fig.6 shows the axes of roll, pitch, and yaw angle and the direction of rotation in the computational model. Equations. (7)-(10) show the four transfer functions used in control.
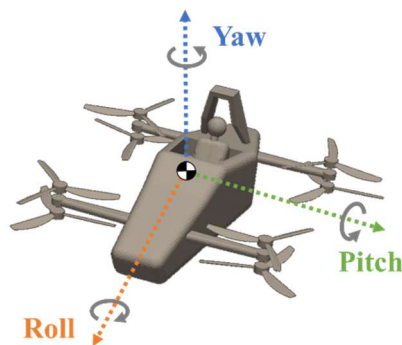

Fig.6   3-axis angle of Flying Car

$$\frac{p(s)}{u_{Roll}} = \frac{LK_T}{I_{xx}s},$$

(7)

$$\frac{q(s)}{u_{Pitch}} = \frac{LK_T}{I_{zz}s},$$

(8)

$$\frac{r(s)}{u_{Yaw}} = \frac{K_A}{I_{yy}s},$$

(9)

$$\frac{v_{lift}(s)}{u_{Throttle}} = \frac{K_T}{ms},$$

(10)

where u_{Roll}, u_{Pitc}, u_{Yaw}, $u_{Throttle}$ are the control inputs for the 3-axis attitude and thrust, p, q, and r are the angular velocities of roll, pitch, and yaw angle, and v_{lift} is the speed in the upward direction. L is the distance of the rotor from the aircraft center of gravity, I is the moment of inertia of the aircraft, K is a coefficient obtained from the lift force and torque [13], and m is the weight of aircraft. Equations. (11)-(13) show the relevant mixing equations. The mixing equation is the ratio of the rotation speed assigned to each rotor from the control input obtained in Equations. (7)-(10).

$$\bar{M} = \begin{bmatrix} 1 & 1 & \cdots & 1 \\ -\bar{r}_{Z1} & -\bar{r}_{Z2} & \cdots & -\bar{r}_{ZN} \\ \bar{r}_{X1} & \bar{r}_{X2} & \cdots & \bar{r}_{XN} \\ e_{p1} & e_{p2} & \cdots & e_{pN} \end{bmatrix},$$

(11)

$$M = \bar{M}^T(\bar{M}\bar{M}^T)^{-1},$$

(12)

$$D = M \begin{bmatrix} u_{Throttle} \\ u_{Roll} \\ u_{Pitc} \\ u_{Yaw} \end{bmatrix},$$

(13)

where $\bar{r}_X$ and $\bar{r}_Z$ are the dimensionless distances from the aircraft center of gravity to the rotor axis of rotation, and e_p is a scalar that defines the direction of rotor rotation, where forward pitch propellers are set to 1 and reverse pitch propellers to -1. D is the number of rotations assigned to each rotor.

4 Calculation results

As shown in Fig.7, each rotor is named FLU, FLL, FRU, FRL, RLU, RLL, RRU, and RRL. The direction of rotor rotation is distinguished by color. The initial letter of each name, such as FLU (Front Left Upper), is used here.
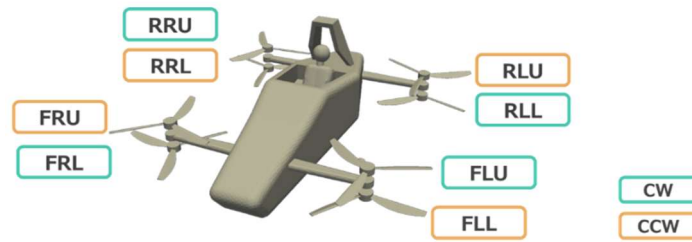

Fig.7 Name of octorotor

4.1 Stopping FLU

Fig.8 shows the results of the sudden stop of one of the FLU rotors. The graphs of eight rotor speed versus time and 3-axis attitude versus time are shown. Before the rotor stops, eight rotors are hovering while maintaining their normal motion and attitude. After the rotor stops, control functions to maintain the attitude with the remaining seven rotors. It can be confirmed that the respective rotor speeds were affected before and after the stop. This is because the FLL, which is positioned below the FLU, is trying to maintain its attitude by increasing its rotation speed through control due to the lack of thrust from the FLU. In order to maintain the 3-axis attitude of the roll-pitch-yaw angle, the rotor speeds of FRL and RLL increased, and the rotor speed of RRL decreased. However, there is a 4[deg] tilt of the pitch angle in the attitude angle, confirming the effect on the aircraft's attitude. The large effect on the roll angle is due to the control gain. The yaw angle was also affected by the torque to the aircraft due to one of the rotors stopping. Therefore, when the rotor stops, the danger of a crash can be avoided by sacrificing one angle because it is difficult to restore all angles to normal.

Fig.9 shows a contour plot of the velocity before and after the rotor stopped suddenly. From Fig.9, the velocity magnitude after the rotor stops increases and the rotor tries to maintain its attitude. It is also confirmed that asymmetric flow in the left/right and front/rear rotors causes instability in the fluid flow on the underside of the flying car. Therefore, it is expected that the flying car will continue to slide sideways while maintaining its current attitude.
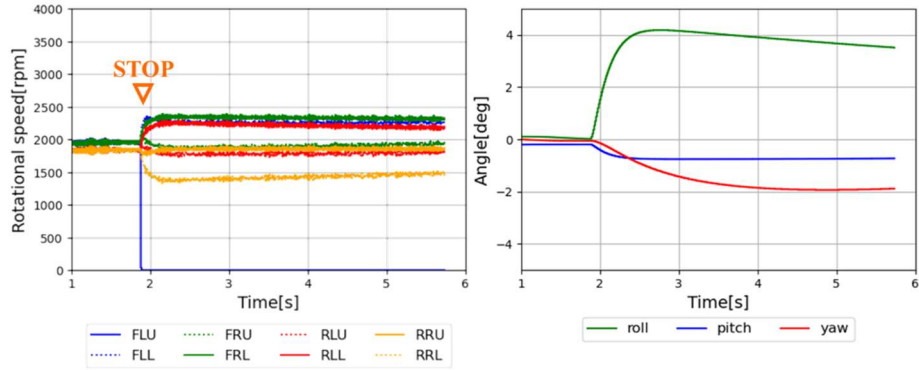
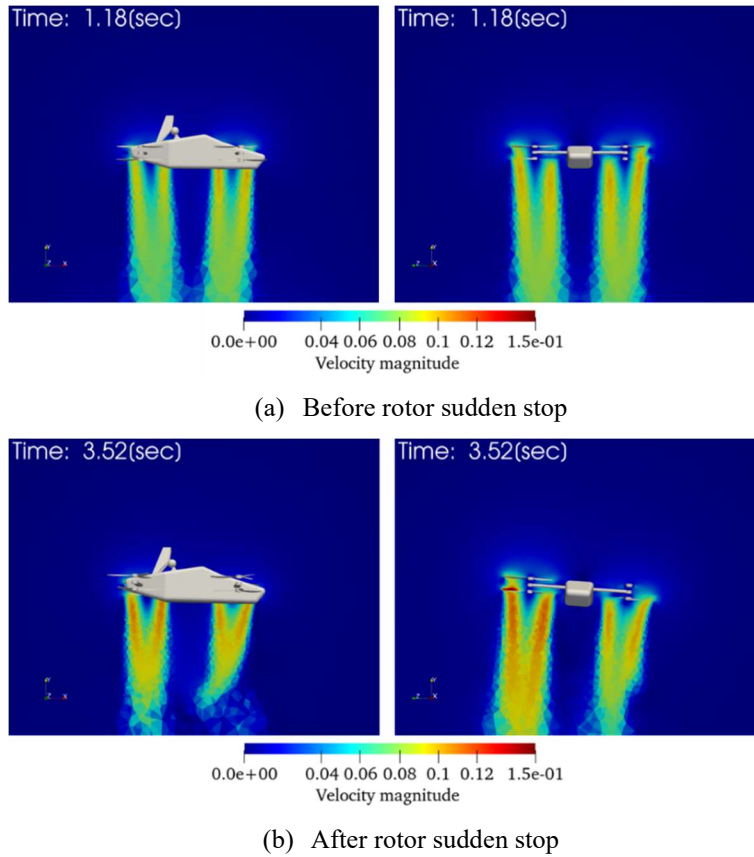**Fig.8** Time histories of rotational speed(rpm) and angle(deg) in FLU stop

(a) Before rotor sudden stop

(b) After rotor sudden stop

Fig.9 Velocity distribution in the plane across the propeller on the left and flont sides at the FLU stop

4.2 Stopping FLU-FLL

This is the result of two contra-rotating rotors, FLU-FLL, stopping simultaneously. Fig.10 shows the trajectory of the flying car at various times due to FLU and FLL sudden stops. Fig.11 shows the isosurface of Q-criterion (Q = 0.01). From Fig.10, the altitude could not be maintained during the FLU-FLL sudden stop, and the flying car crashed while rotating. At this time, the lift force suddenly is lost from one rotor, causing the rotor to lose its attitude, and the other six rotors could not recover.

From Fig.11, it can be confirmed that the entire body is caught in the vortex after the rotor suddenly stops. As a result, the aircraft could not maintain its attitude by control and crashed. Considering the balance of forces on the aircraft, it is necessary to operate the rotors of the RRU-RRL, which are located diagonally opposite to the stopped rotor, in a new way.
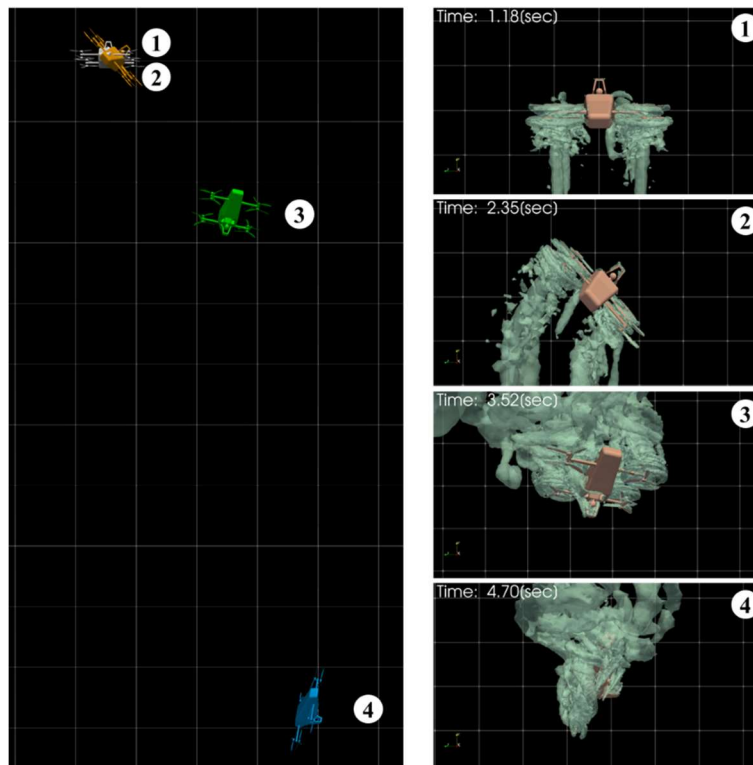

Fig.10　Time histories of position y-z in FLU-FLL stop (left)

Fig.11　Isosurfaces of Q-criterion (Q = 0.01) at FLU-FLL stop (right)

4.3   No Rotation Speed Limit in Stopping FLU-FLL

When the FLU-FLL was stopped, the aircraft's attitude significantly collapsed and the aircraft crashed. This was considered to be due to a decrease in lift force from one side. Therefore, to balance the forces applied to the aircraft, the control method of the rotor located at the opposite angle was changed. The direction of rotation of the rotor is determined by its shape. However, we thought that it would be possible to obtain a negative lift force by turning the rotor in the opposite direction. Therefore, we made it possible to rotate in the opposite direction by eliminating the lower limit of the rotation speed control. Two of the FLU-FLL are stopped, but the rotation speed limit for each rotor is eliminated to allow reverse rotation. Fig. 12 shows graphs of 8 rotor speed versus time and 3-axis attitude versus time. The graphs in Fig.8 and Fig.12 compare the results when the rotor speed limit is 0-4000 [rpm] and when the rotor speed is not limited as shown in Fig.8 and Fig.12, respectively. From Fig.12, it can be confirmed that the rotation of RRU-RRL (yellow line), which is located diagonally, shifts to the reverse direction as soon as the rotation of FLU-FLL stops. The reverse rotation of the rotors generates thrust in the reverse direction of the normal rotation, which enables the flying car to maintain its 3-axis attitude angle and maintain its altitude without crashing. By enabling reverse rotation of the rotor and obtaining reverse thrust, it is possible to approach stable flight.

   Fig.13 shows the isosurfaces of Q-criterion (Q = 0.01) with FLU-FLL sudden stops and no speed limit. As shown in Fig.13, the reverse rotation confirms that the fluid flows in the opposite direction to the normal direction and produces the opposite thrust.
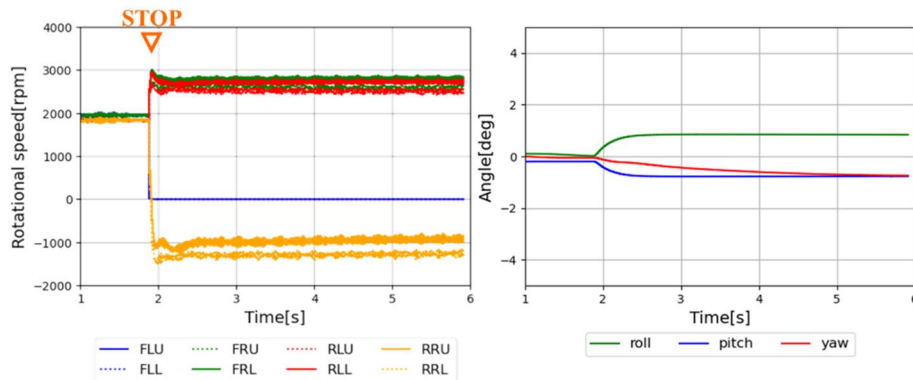

Fig.12   Time histories of rotational speed(rpm) and angle in FLU-FLL stop (No limit)
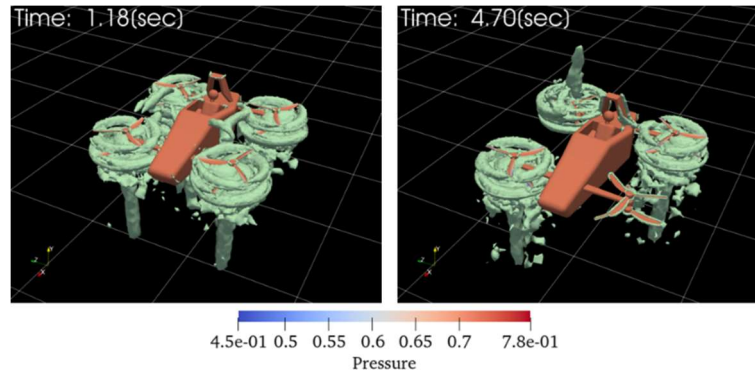
Fig.13 Isosurfaces of Q-criterion (Q = 0.01) at FLU-FLL stop (No Limit)

Fig.14 shows the difference in lift force between forward and reverse rotation depending on the rotor geometry used in this study. The vertical axis is the lift force, and the horizontal axis is the rotation speed. The results show that reverse rotation results in a negative lift force value compared to normal rotation. These results indicate that reverse rotation at the appropriate timing can reduce the hazardous behavior of the rotor when it comes to a sudden stop.
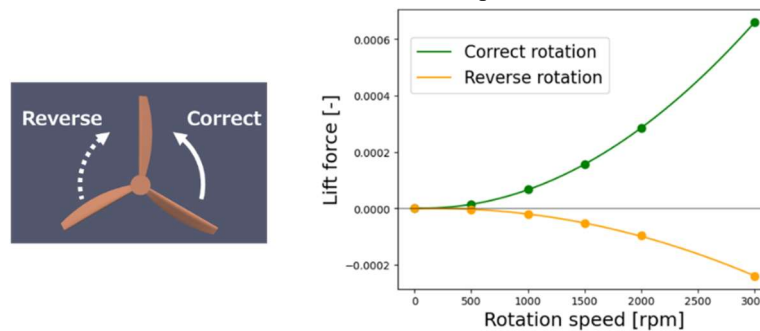

Fig.14 Difference in lift force between correct and reverse rotation speeds

5   Conclusions

A 6-degrees of freedom flight simulation of an octorotor flying car with a sudden rotor stop was performed by calculating the coupling of fluid and rigid-body interactions. The MCD method based on the unstructured moving mesh finite volume method and the multi-axis sliding mesh method were combined as the computational method. In the simulation of the rotor sudden stop, one and two of the eight rotors were stopped, and the rotation speed assignment was evaluated based on the obtained 3-axis attitude of the flying car. It was confirmed that a one-rotor stop affects the attitude of the flying car, but is unlikely to cause a dangerous situation such as a crash. However, the two-rotor stop may cause a crash depending on the arrangement of the

rotors, and it was found that countermeasures were necessary. Therefore, reverse rotation is possible in a rotor that has not stopped. The reverse rotation was confirmed to stabilize the attitude of the flying car by obtaining thrust in the opposite direction of the normal rotation. In the future, we would like to be able to investigate aircraft behavior with other propeller stop and evaluate safety for many different aircraft models.

References

1. Alessandro, B. *et al.*: Electric VTOL Configurations Comparison. Aerospace, Volume 6, Issue 3 (2019)
2. Barcelos, D. *et al.*: Experimental study of the aerodynamic loads on the airframe of a multirotor UAV. 65th Aeronautics Conference, CASI AERO 21 (2021)
3. Seokkwan, Y. *et al.*: Computational Study of Flow Interactions in Coaxial Rotors (2016)
4. Alberto, S. *et al.*: A Technocritical Review of Drones Crash Risk Probabilistic Consequences and its Societal Acceptance (2015)
5. Watanabe, K. *et al.*: Moving computational domain method and its application to fow around a highspeed car passing through a hairpin curve. J Comput Sci Technol 3(2):449–459 (2009)
6. Takii, A. *et al.*: Six degrees of freedom numerical simulation of tilt-rotor plane. ICCS2019, Faro. Lecture notes in computer science, vol 11536. Springer, Cham, pp 506–519 (2019)
7. Yamakawa, M. *et al.*: Numerical Simulation of Free Surface Affected by Submarine with a Rotating Screw Moving Underwater, ICCS 2021, LNCS 12747, pp 268–281 (2021)
8. Roe PL, Approximate Riemann solvers, parameter vectors, and diference schemes. J Comput Phys 43(2):357–372 (1981)
9. Hishida, M. *et al.*: A new slope limiter for fast unstructured CFD solver FaSTAR. In: Proceedings of 42nd fuid dynamics conference / aerospace numerical simulation symposium. Japan Aerospace Exploration Agency, JAXA-SP-10-012, pp 85–90 (in Japanese) (2010)
10. SkyDrive Inc Homepage. https://en.skydrive2020.com/. Accessed 23 Jan 2023
11. Ito, Y. *et al.*: Surface triangulation for polygonal models based on CAD data. Int J Numer Methods Fluids 39(1):75–96 (2002)
12. Ito Y, Challenges in unstructured mesh generation for practical and efcient computational fuid dynamics simulations. Comput Fluids 85(1):47–52 (2013)
13. Gomi, R. *et al.*: Flight simulation from takeof to yawing of eVTOL airplane with coaxial propellers by fuid-rigid body interaction (2023)